


# Approach for the probabilistic fatigue assessment of welded joints based on the local geometry of the weld seam

Jan Schubnell<sup>1</sup> | Sai Kumar Konidena<sup>1</sup> | Matthias Jung<sup>1</sup> | Moritz Braun<sup>2</sup>  |  
Sören Ehlers<sup>2</sup> | Mauro Madia<sup>3</sup> | Thomas Kannengießer<sup>3</sup> | Daniel Löschner<sup>4</sup>

<sup>1</sup>Fraunhofer Institute for Mechanics of Materials IWM, Freiburg, Germany

<sup>2</sup>DLR Institute of Maritime Energy Systems, Geesthacht, Germany

<sup>3</sup>BAM-Federal Institute for Materials Research and Testing, Berlin, Germany

<sup>4</sup>University of Applied Sciences Munich, Munich, Germany

## Correspondence

Jan Schubnell, Fraunhofer Institute for Mechanics of Materials IWM, Woehlerstr. 11, 79108 Freiburg, Germany.

Email: [jan.schubnell@iwmm.fraunhofer.de](mailto:jan.schubnell@iwmm.fraunhofer.de)

## Abstract

Welded joints show large variation of the weld toe geometry along the weld seam, which is one important reason for the comparably large scatter in fatigue life. Therefore, it is crucial to take the local geometry at the weld toe into account, to reduce the conservatism in fatigue assessment of welded joints. This study is based on the IBESS procedure for the calculation of the fatigue strength, whereby the evaluation of local geometrical parameters is carried out by means of 3D surface scans. The approach is validated against 26 fatigue test series. The fatigue life is in general overpredicted, whereas good agreement is achieved for high stress ratio ( $R = 0.5$ ). A sensitivity analysis conducted with IBESS shows that weld toe radii  $\rho < 2$  mm and flank angle  $\alpha < 30^\circ$  have a significant influence on the calculated fatigue strength. In contrast to this, no strong correlation between  $\rho$  and the fatigue strength was determined experimentally in this study.

## KEYWORDS

3D scanning, fatigue strength, fracture mechanics, IBESS approach, local weld geometry, welded joints

**Abbreviations:**  $A$ , coefficient in the cyclic  $R$ -curve power law;  $a$ , crack depth (mm);  $a_0$ , El-Haddad parameter (mm);  $a_i$ , initial crack depth (mm);  $a_{LC}$ , transition crack length from short- to long-crack growth regime (mm);  $b$ , exponent in the cyclic  $R$ -curve power law;  $C$ , constant in the Paris–Erdogan law (given for  $da/dN$  in mm/cycle and  $\Delta K$  in  $\text{MPa mm}^{1/2}$ );  $C_B$ , constant in the Basquin-law;  $E$ , Young's modulus (MPa);  $\hat{E}(X)$ , estimation of the expected value of the statistical distribution; FAT, fatigue class according to the IIW recommendation (MPa);  $h$ , weld reinforcement height (mm);  $k$ , slope of the  $S$ – $N$  curve;  $K'$ , Ramberg–Osgood coefficient (MPa);  $L$ , weld leg length (mm);  $m$ , exponent in the Paris–Erdogan law;  $N$ , number of load cycles;  $n'$ , Ramberg–Osgood exponent;  $P$ , cumulative probability (%);  $P_f$ , failure probability (%);  $R$ , stress ratio;  $R_m$ , tensile strength (MPa); SCF, stress concentration factor;  $t$ , secondary notch depth (mm);  $T$ , plate thickness (mm);  $T_N$ , scatter range;  $W$ , plate width (mm);  $\alpha$ , flank angle ( $^\circ$ );  $\Delta K$ , stress intensity factor range ( $\text{MPa mm}^{1/2}$ );  $\Delta K_{th,eff}$ , intrinsic fatigue crack propagation threshold ( $\text{MPa mm}^{1/2}$ );  $\Delta K_{th,LC}$ , fatigue crack propagation threshold (long-crack regime) ( $\text{MPa mm}^{1/2}$ );  $\Delta S$ , nominal stress range (MPa);  $\Delta S_{2.5\%}$ , nominal stress range at  $2 \times 10^6$  load cycles of  $P_f = 2.5\%$  (MPa);  $\Delta S_{50\%}$ , nominal stress range at  $2 \times 10^6$  load cycles of  $P_f = 50\%$  (MPa);  $\Delta\sigma_e$ , fatigue limit (stress range) (MPa);  $\kappa$ , curvature (mm);  $\hat{\mu}$ , estimation of the first parameter of the statistical distribution;  $\rho$ , weld toe radius (mm);  $\hat{\sigma}$ , estimation of the second parameter of the statistical distribution (standard deviation);  $\sigma_e$ , fatigue limit (stress amplitude) (MPa);  $\sigma_m$ , mean stress (MPa);  $\hat{\sigma}_X$ , estimation of the standard deviation of the statistical distribution.

This is an open access article under the terms of the [Creative Commons Attribution](https://creativecommons.org/licenses/by/4.0/) License, which permits use, distribution and reproduction in any medium, provided the original work is properly cited.

© 2023 The Authors. *Fatigue & Fracture of Engineering Materials & Structures* published by John Wiley & Sons Ltd.

### Highlights

- Direct consideration of the geometry of welded joints for probabilistic fatigue life assessment.
- Fatigue life assessment considering physical short and long cracks.
- Correlation of fatigue life and weld toe geometry.
- Statistical analysis of geometrical parameters for 26 fatigue test series.

## 1 | INTRODUCTION

The fatigue strength of welded joints is low compared with the corresponding fatigue strength of the base material. For this reason, welded joints are weak points in welded industrial parts and constructions. In most cases, the geometrical notches at the weld toe are structural weak points of the welded joints in steel constructions if inner defects are avoided or are small. The low fatigue strength at the weld toe in steel joints is related to the coarse-grain microstructure of the heat-affected zone (HAZ),<sup>1</sup> local tensile residual stresses caused by cooling and shrinkage,<sup>2</sup> and the stress concentration of the geometrical notch.<sup>3</sup> The fatigue design of welded joints follows a total-life or fracture mechanics approach according to the current recommendations.<sup>4–7</sup> Due to large scatter of the parameters governing the fatigue life, and to the aim of ensuring a safe design, usually lower bounds for the material fatigue resistance and upper bounds for the applied loads are used. This, together with simplified modeling hypotheses, can lead to conservative design, typically large sheet thicknesses in fatigue-loaded welded structures. A full probabilistic fatigue approach goes beyond the deterministic evaluation of lower and upper bounds of the input variables. The use of statistical distributions for the description of the weld geometry is beneficial to the thorough understanding of the variables influencing the scatter in fatigue lives. This would help in the interpretation of outliers in case of large deviations in the weld toe geometry and potentially to decrease the conservatism of current deterministic approaches.

Several studies have shown that the fatigue strength of welded joints is directly related to the local geometry along the weld seam.<sup>3,8–16</sup> The local geometry of the weld toe is described by the weld toe radius  $\rho$ , flank angle  $\alpha$ , and depth of the secondary notch or undercut  $t$ . These account for the stress concentration at the weld toe (notch effect). Recent studies have shown that fatigue crack starts from single locations with high stress concentrations given typically by low weld toe radii or deep undercuts.<sup>17–19</sup> Thus, the local weld toe geometry usually

shows a high variation<sup>20</sup> and is related to a high number of factors during arc welding, for example, the torch position, welding technique and welding parameters, number of layers, type of welded joint and weld detail, and skills of the operator.<sup>21</sup>

The assessment of the weld quality in quality groups—B, C, and D according to DIN EN ISO 5817:2014<sup>22</sup> or ISO 6520-1:2007<sup>23</sup> or VB, VC, and VD according to Volvo STD 181-0004<sup>24</sup>—is related to single geometrical parameters like the weld toe radius, flank angle, or height of the weld bead. Thus, the Eurocode standards DIN EN 1993-1-9<sup>5</sup> and DIN EN 1999-1-1<sup>25</sup> do not take local geometrical parameters of weld toe into account; their influence is included in the fatigue design curves. Other guidelines for fatigue design of welded joints<sup>4,5,7</sup> cover geometrical parameters, for example, the height of the weld bead or weld reinforcement, and relate these to individual fatigue classes. In general, the given fatigue classes in these guidelines cover the geometrical variations by high conservatism. It is also important to mention that none of the mentioned standards give recommendations regarding the measurement of the geometrical parameters.

The main goal of the current study is a validation of a comprehensive procedure for the fatigue life assessment of welded joints based on local geometrical parameters (see Figure 1). This procedure is not new and is mainly adopted from previous work by the IBESS cluster,<sup>1,16,17,26</sup> even though some major differences regarding the input parameters exist. In fact, in this study, some important material parameters were not known and have been estimated according to empirical rules or guidelines. Furthermore, it is important to mention that the application of the IBESS procedure to the assessment of the fatigue strength of weldments resulted in any case conservative compared to the experimental tests so far (see Madia et al.<sup>17</sup>).

Further aim is to correlate the fatigue life of welded joints with the local geometrical parameters in a similar fashion to the sensitivity analyses proposed in Schork et al.<sup>16</sup>

The proposed procedure includes the digitalization of the surfaces of welded joints by 3D scanning, the

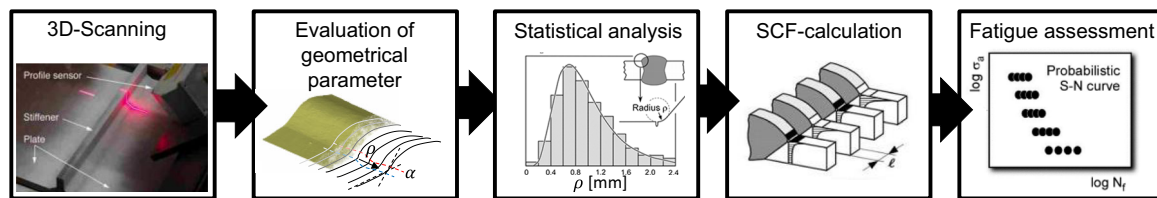


**FIGURE 1** Process chain for the probabilistic fatigue life assessment of welded joints based on their individual geometry. [Colour figure can be viewed at [wileyonlinelibrary.com](http://wileyonlinelibrary.com)]

evaluation of the geometrical parameters, the statistical analysis of these parameters, the calculation of stress concentration and stress through-thickness distributions, and, finally, the probabilistic fatigue life assessment. The current study is based on former work regarding 3D scanning of welded joints by Schubnell et al.<sup>20</sup> and Renken et al.<sup>27</sup> (3D scanning and evaluation of geometrical parameters), Braun et al.<sup>28</sup> (statistical analysis), Kiyak et al.<sup>29</sup> (SCF calculation), Madia et al.,<sup>17</sup> and Zerbst et al.<sup>26</sup> (probabilistic fatigue life assessment). For the reasons mentioned, it is necessary to include the local geometry at the weld toe in fatigue assessment methods to improve the accuracy of fatigue life predictions and reduce the conservatism in the current recommendations. The development of the IBESS approach<sup>17,26</sup> includes the statistical description of the local weld toe geometry for probabilistic fracture mechanics analysis of welded joints. This probabilistic approach is based on statistical distribution of the geometrical parameters of welded joints. The current study is based on fatigue data from previous investigations (see Section 2), briefly describes the determination and statistical evaluation of the geometrical parameters (see Section 3), and outlines the statistical analysis of fatigue tests (see Section 4). The fatigue assessment by the IBESS approach is described in Section 5, and the correlation between the geometrical parameters and the fatigue strength of welded joints is investigated in Section 6.

## 2 | MATERIALS AND SPECIMENS

The geometrical parameters and fatigue test results taken from previous studies<sup>30–36</sup> and other unpublished investigations are summarized in Table 1. These data contain 390 single fatigue tests with four different types of welded joints: single V-butt joints, double V-butt joints, cruciform joints, and T-joints. The plate thickness ranges from 6 to 20 mm. All welded joints were made of structural steels S235, AH36, S355, S500, and S960. The welded specimens were produced by submerged arc welding (SAW), flux-cored arc welding (FCAW), laser and laser-hybrid welding, and gas metal arc welding (GMAW).

## 3 | LOCAL WELD GEOMETRY

### 3.1 | Definition

Geometrical parameters of welding joints are defined in several weld quality standards, for example, ISO 5817,<sup>22</sup> Volvo STD,<sup>24</sup> International Institute of Welding (IIW) guideline,<sup>4</sup> or Eurocode 3,<sup>5</sup> and others that relate also single geometrical parameters to the fatigue strength of welded joints. Numerous investigations have indicated that one of the most critical factors affecting the fatigue life of welded joints is the variable geometry of the 2D weld cross-sections, defined by the geometrical parameters according to previous investigations.<sup>29,37–39</sup> The geometrical parameter used in this study for different weld types is shown in Figure 2. Parameters that define misalignment of the weld (e.g., the distortion angle) are not considered in this study. However, the additional stresses generated by macroscopic imperfections (distortion of the mounting process) maybe more important than the effect of the local weld geometry in large assemblies. For the following investigations, the geometrical parameters are divided into those that define the shape of the weld detail (leg length  $L$ , weld reinforcement height  $h$ , and plate thickness  $T$ ) and those that define the local notch geometry at the weld toe (weld toe radius  $\rho$ , flank angle  $\alpha$ , and depth of the secondary notch [or undercut]  $t$ ).

### 3.2 | Determination of the local weld geometry by 3D scanning

The geometrical parameters in this work are characterized for 15 different welded joints A to O, summarized in Table 1, and four different weld details, illustrated in Figure 2. The surface of the welded joints is digitalized by laser scanning profilometry (LSP) (series A to G and O) and by stripe light projection (SLP) (series I to N). However, for all series, the same evaluation algorithm, the curvature method developed by Jung,<sup>41</sup> was used. The curvature method was later improved by Renken et al.<sup>27</sup> Previous studies have shown that the curvature algorithm was relatively robust and is able to determine

TABLE 1 Overview of fatigue test series.

Name	Base material	Welding process	Weld type	Load ratio $R$ (-)	Load type	Number of specimens	Fatigue strength <sup>a</sup> (MPa)		Slope $k$ (-)	Ref.
							$k = 3$	$k = \text{free}$		
A1	S235	FCAW	Single	0	T	30	77	86	2.69	30
B1	S355	LH	Single	0.5	T	10	124	83	5.98	31
B2	S355	LH	Single	0	T	26	125	94	4.23	31
C1	A36	SAW	Double	-1	T	21	99	97	3.12	31
C2	A36	SAW	Double	0	T	20	101	79	4.23	31
D1	A36	SAW	Double	0	T	24	70	63	3.37	31
D2	A36	SAW	Double	0.5	T	25	85	74	3.95	31
E1	S355	SAW	Single	0.5	T	22	71	75	2.49	30
E2	S355	SAW	Single	0	T	20	106	82	4.07	30
F1	S355	SAW	Single	0.5	T	10	81	84	2.64	32
F2	S355	SAW	Single	0	T	24	79	89	2.53	32
F3	S355	SAW	Single	-1	T	15	111	123	2.51	32
G1	S500	FCAW	Single	0	T	13	137	117	3.56	30
G2	S500	FCAW	Single	0.5	T	21	72	74	2.87	30
H1	S960QL	GMAW	Cruciform	0.1	B	10	169	108	4.34	33,35
H2	S960QL	GMAW	Cruciform	0.5	B	10	138	117	3.68	35
I1	S960QL	GMAW	Cruciform	0.1	B	9	210	127	4.69	35
I2	S960QL	GMAW	Cruciform	0.5	B	9	159	100	5.36	35
J1	S355J2	GMAW	Cruciform	0.1	B	8	157	123	3.92	33,35
J2	S355J2	GMAW	Cruciform	0.5	B	8	127	120	3.31	35
K1	S355J2	GMAW	Cruciform	0.1	B	7	225	150	5.22	35
K2	S355J2	GMAW	Cruciform	0.5	B	7	156	116	5.05	35
L1	S960QL	GMAW	Cruciform	0.1	T	10	93	82	3.34	34
M1	S355J2	GMAW	Cruciform	0.1	T	11	95	86	3.29	34
N1	S355J2	GMAW	Single	0.1	T	10	145	117	3.86	36
O1	S355M	GMAW	T-joint	0.1	T	14	182	154	3.55	

Note: Single, single V-butt joint; Double, double V-butt joint; Cruciform, cruciform joint; T, tension; B, bending.

<sup>a</sup>Evaluated at  $2 \times 10^6$  load cycles and  $P_f = 2.5\%$ .

the weld toe in a sufficient way with a wide range of industry standard measurement solution.<sup>20</sup> The point distance of the used measurement systems is  $\approx 0.025$  mm/pts.

### 3.3 | Statistical analysis

The use of the probabilistic fracture mechanics approach for fatigue life assessment (see Section 5) requires the theoretical statistical distribution of the local geometrical parameters. Most commonly used theoretical statistical distributions are summarized in Table 2 according to

previous investigations.<sup>17,26</sup> The most significant parameters are the weld toe radius  $\rho$ , the flank angle  $\alpha$ , and the secondary notch depth  $t$  according to Zerbst et al.<sup>26</sup> The geometrical variation of the global geometrical parameters of leg length  $L$ , weld reinforcement height  $h$ , and plate thickness  $T$  was neglected in this study. Studies by Renken et al.<sup>27</sup> showed that the variation of  $L$  is low compared with  $\rho$  and  $\alpha$ . Investigations by Braun et al.<sup>28</sup> showed that it is difficult to determine suitable distribution functions for the investigated weld geometry parameters ( $\rho$ ,  $\alpha$ ,  $L$ ,  $h$ , and  $t$ ). The slight skewness of the distribution of the flank angle  $\alpha$  allows the assumption that a normal distribution can be used, even if high

**FIGURE 2** Geometrical parameters of different weld details: (A) single V-butt joint, (B) double V-butt joint, (C) T-joint, and (D) cruciform joint.<sup>3,40</sup> [Colour figure can be viewed at [wileyonlinelibrary.com](http://wileyonlinelibrary.com)]

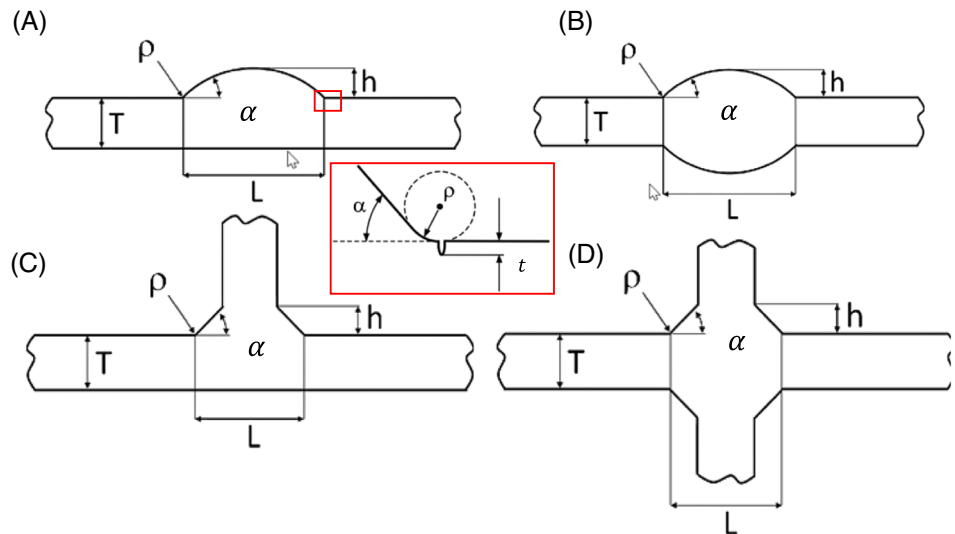


**TABLE 2** Characteristics of the statistical distribution functions used in this study.

	Normal distribution (N)		Log-normal distribution (LN)	
CDF	$P(x) = \Phi\left(\frac{x-\mu}{\sigma}\right)$	(1)	$P(x) = \Phi\left(\frac{\ln(x)-\mu}{\sigma}\right)$	(2)
Parameter estimation	$\hat{\mu} = \frac{1}{n} \sum_{i=1}^n X_i$	(3)	$\hat{\mu} = \frac{1}{n} \sum_{i=1}^n \ln(X_i)$	(4)
	$\hat{\sigma}^2 = \frac{1}{n-1} \sum_{i=1}^n (X_i - \hat{\mu})^2$	(5)	$\hat{\sigma}^2 = \frac{1}{n-1} \sum_{i=1}^n (\ln(X_i) - \hat{\mu})^2$	(6)
Mean and variance	$\hat{E}(X) = \hat{\mu}$	(7)	$\hat{E}(X) = \exp\left(\hat{\mu} + \frac{\hat{\sigma}^2}{2}\right)$	(8)
	$\hat{\sigma}_X = \sqrt{\hat{\sigma}^2}$	(9)	$\hat{\sigma}_X = \sqrt{(\exp(\hat{\sigma}^2) - 1) \cdot \exp(2\hat{\mu} + \hat{\sigma}^2)}$	(10)

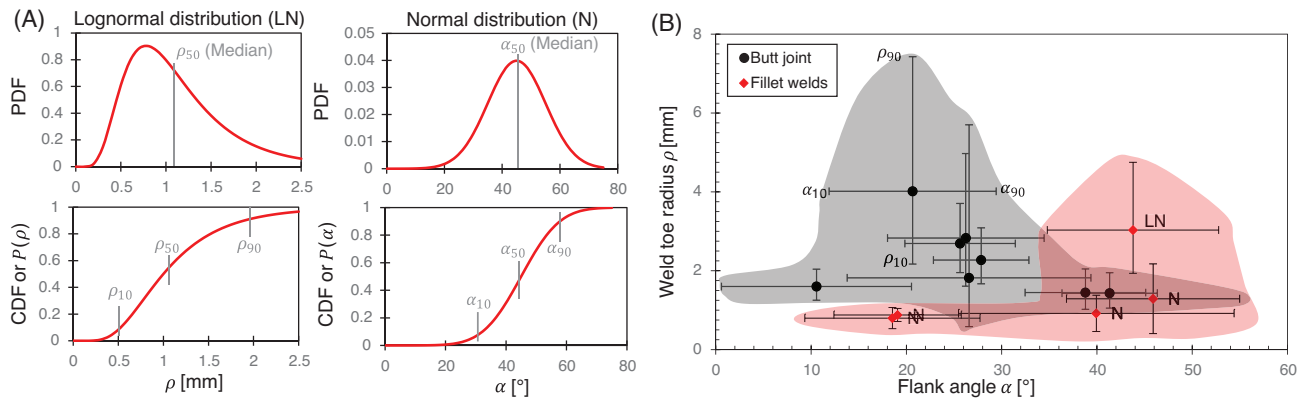


**FIGURE 3** Statistical treatment of the geometrical parameters: (A) statistical distributions of weld toe radius  $\rho$  and flank angle  $\alpha$  and (B) overview of the evaluated geometrical parameters given in Table 3. [Colour figure can be viewed at [wileyonlinelibrary.com](http://wileyonlinelibrary.com)]

kurtosis that means the tail of the real distribution of  $\alpha$  is wider.<sup>28</sup> The corresponding cumulative density function (CDF) is given in Table 2 (see Equation 1). The weld toe radii seem to follow a skewed log-normal distribution,<sup>3,16,28,42</sup> with a CDF given in Table 2 (see Equation 2). Examples of the statistical distribution

functions of CDF and probability density function (PDF) of the geometrical parameters are illustrated in Figure 3A. For the secondary notch depth  $t$ , different methods of determination are given (see Section 5.1.2). Braun et al.<sup>28</sup> showed that the determination of  $t$  by 3D scans leads to highly skewed distributions because of the



TABLE 3 Weld geometry of the specimens used in the fatigue tests.

Test series	Weld toe radius $\rho$			Flank angle $\alpha$		Weld attachment length $L$ (mm)	Weld reinforcement $h$ (mm)	Plate width $W$ (mm)	Plate thickness $T$ (mm)
	$\hat{E}(X)$	$\hat{\sigma}_X$	Distribution	$\hat{E}(X)$	$\hat{\sigma}_X$				
	(mm)	(mm)		(°)	(°)				
A1	3.12	1.44	LN	26.24	6.41	12.8	2.0	40	10
B1, B2	2.71	2.98	LN	26.58	9.98	3.9	0.5	40	6
C1, C2	1.50	0.41	LN	38.79	4.94	33.5	4.5	40	20
D1, D2	1.48	0.36	LN	41.33	3.90	21.2	3.4	40	12
E1, E2	2.78	0.71	LN	25.64	4.52	18.2	2.0	40	10
F1, F2, F3	2.34	0.57	LN	27.85	3.91	23.1	1.8	40	16
G1, G2	4.51	2.29	LN	20.66	6.84	19.8	1.5	40	10
H1, H2	1.29	0.69	N	45.89	7.10	15.7	2.8	130	10
I1, I2	0.88	0.13	N	19.08	5.21	25.1	2.8	130	10
J2, J2	0.92	0.36	N	39.93	11.28	15.6	2.8	130	10
K1, K2	0.80	0.21	N	18.54	7.17	25.1	2.8	130	10
L1	1.29	0.69	N	45.89	7.09	15.6	2.8	50	10
M1	0.92	0.36	N	39.93	11.28	15.6	2.8	50	10
N1	1.63	0.31	LN	10.57	7.78	12.8	2.0	50	10
O1	3.23	1.16	LN	43.78	7.02	31.3	5.7	60	20

Note: Flank angle is always in normal distribution.

Abbreviations: LN, log-normal distribution; N, (Gaussian) normal distribution.

very small shape of  $t$  compared with the resolution of the measurement system. However, the determination of  $t$  based on roughness profiles<sup>26</sup> leads to nearly symmetrical distributions.<sup>43</sup> In this work, normal distributions are used for the description of  $t$ .

The values for mean  $\hat{E}(X)$  and variance  $\hat{\sigma}_X$  of the estimated probability distributions for test series A to O are summarized in Table 3 (note the different definitions for normal and log-normal distributions, see Equation 3 to 10 in Table 2). For measurements performed by Schubnell et al.,<sup>20</sup> the determined normal distributions were used for  $\rho$ . For newer evaluations, log-normal distributions were used to describe  $\rho$ , and normal distributions were used for  $\alpha$  and  $t$ , with their characteristic parameters given in Table 2. The range of the geometrical parameters  $\rho$  and  $\alpha$  is illustrated in Figure 3B and shows that a large overlap between butt joints and fillet welds exists. The displayed scatter ranges from a cumulative

probability of  $P=10\%$  to  $P=90\%$  (written as  $\rho_{10}$ ,  $\rho_{90}$ ,  $\alpha_{10}$ , and  $\alpha_{90}$ ); see Figure 3A for illustration. As shown, the weld toe radii range from around 0.2 to 2.5 mm and the flank angles range from  $2^\circ$  to  $56^\circ$ . As expected, the mean values for the flank angle are higher for fillet welds than for butt joints. However, test series I and K are multi-layer welded joints and show a comparably low flank angle for fillet welds.

#### 4 | EXPERIMENTAL FATIGUE STRENGTH DETERMINATION

Fatigue test data from all the test series mentioned in Table 1 were reevaluated according to DIN 50100-2016-12<sup>44</sup> using the pearl string method. The  $S-N$  curve with a survival probability of 50% is calculated from the data by performing a linear regression of

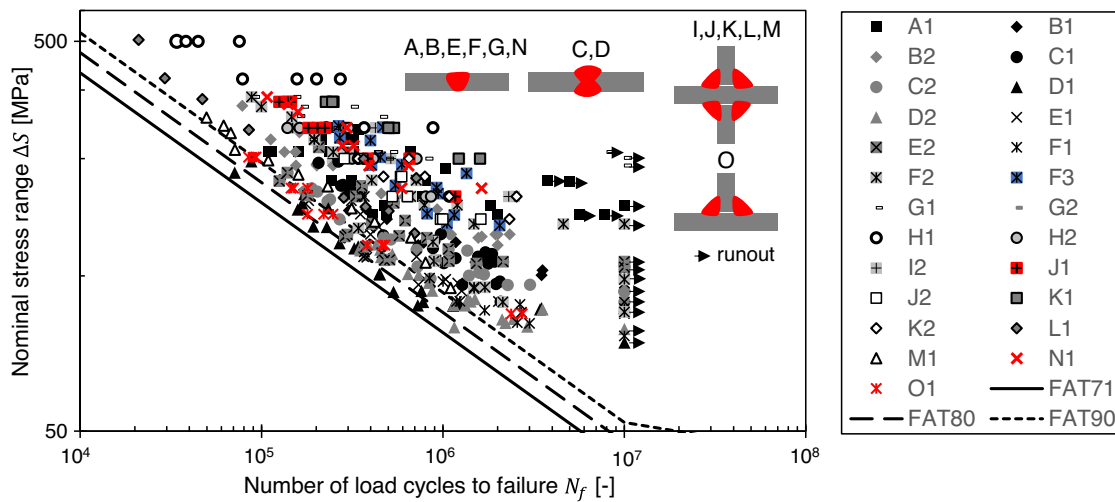


FIGURE 4 Overview of fatigue test data. [Colour figure can be viewed at [wileyonlinelibrary.com](https://onlinelibrary.wiley.com/doi/10.1111/ffe.1470)]

Equation (11) for  $C_B$  and  $k$ , with  $N$  being the dependent variable:

$$\log(N) = \log(C_B) - k \cdot \log(\Delta S). \quad (11)$$

The scatter is analyzed by projecting the data points parallel to the obtained  $S-N$  curve onto a common fictitious load level  $\Delta S_{fict}$ , which gives a set of fictitious fatigue life values  $N_{i,fict}$ . An estimation of the standard deviation is calculated in Equation (12), using a correction as suggested by DIN 50100, with  $n$  being the number of tests in the test series.

$$\tilde{s}_{\log N, corr} = \sqrt{\frac{1}{n-2} \cdot \sum \left( \log N_{i,fict} - \frac{1}{n} \sum \log N_{i,fict} \right)^2} \cdot \frac{n-1.74}{n-2}. \quad (12)$$

The scatter value  $T_N$  is calculated from the standard deviation using Equation (13):

$$T_N = 10^{2.564 \cdot \tilde{s}_{\log N, corr}}. \quad (13)$$

As a characteristic value for the fatigue strength of a test series, the 2.5% failure probability stress range at  $2 \cdot 10^6$  cycles  $\Delta S_{2.5\%}$  is calculated using Equation (14), where  $-1.96$  is the 2.5% quantile of the standard normal distribution.

$$\Delta S_{2.5\%} = \Delta S_{fict} \cdot \left( \frac{2 \cdot 10^6}{10^{\frac{1}{k} \sum \log N_{i,fict} - 1.96 \cdot \tilde{s}_{\log N, corr}}} \right)^{-\frac{1}{k}}. \quad (14)$$

The database of this study is shown in Figure 4 and contains 26 test series with 14 different welded joints and 390 single fatigue tests (excluding runouts). The evaluated fatigue strength, according to the nominal stress approach and the inverse slope of the  $S-N$  curves, is given in Table 1. The characteristic fatigue strengths  $\Delta S_{2.5\%}$  range from 71 to 225 MPa and cover a large range of the FAT classes in the current version of the IIW recommendation,<sup>4</sup> even if only welded joints in as-welded condition are used for evaluation. The used failure criterion was the final fracture of the specimen or loss of specimen stiffness that correlates with extensive crack depth (close to the thickness of the specimen).

## 5 | PROBABILISTIC FRACTURE MECHANICS ANALYSIS

Numerous studies have shown that the fatigue life of the majority of materials under axial loading conditions is mostly spent in the period of fatigue crack propagation, especially if the material state contains defects like geometrical discontinuities (and obviously also for welded joints).<sup>26</sup> For these reasons, the fatigue life assessment of welded joints is carried out using fracture mechanics approaches assuming no, or a relatively short, crack initiation phase. Probabilistic fracture mechanics concepts can be used to describe the crack propagation in material conditions where the stress concentrations (and the geometrical discontinuous or defects) are randomly distributed, as is assumed in the base for welded joints.

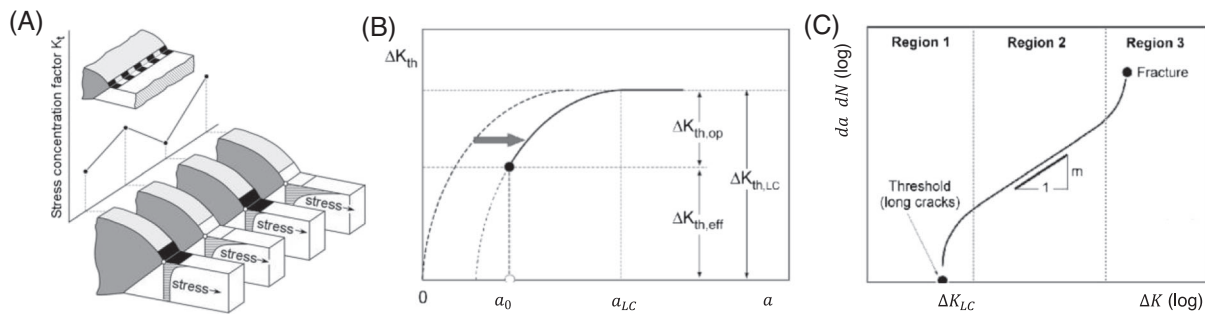


FIGURE 5 Schematic of modeling assumptions: (A) modeling of weld geometry,<sup>17</sup> (B) evolution of the fatigue crack propagation threshold in the short-crack regime, and (C) fatigue crack propagation rate in the long-crack regime as given in the IBESS approach.<sup>40</sup>

## 5.1 | The IBESS approach

The acronym IBESS stands for “Integrale Bruchmechanische Ermittlung der Schwingfestigkeit von Schweißverbindungen” which, translated from the German, means “integral fracture mechanics determination of the fatigue strength of welds.”<sup>26</sup> This method was developed by the German IBESS research cluster to cover the basic mechanism and novel aspects of fatigue failure of welded joints: crack propagation of mechanical/physical short cracks, the phenomena of crack closure, meaningful definition of the initial crack size, multiple crack propagations and coalescence between multiple cracks, and the variation of the weld toe geometry, to mention the most important ones. For detailed description, the reader may refer to Zerbst et al.<sup>26</sup> or Madia et al.<sup>17</sup>

### 5.1.1 | Modeling of the weld geometry

The modeling strategy adopted in the IBESS approach is based on partitioning the weld toe in a finite number of equidistant sections to reproduce the variation of the local geometrical parameters, as shown in Figure 5A. The weld toe radius  $\rho$ , the flank angle  $\alpha$ , and the depth of the secondary notch  $t$  have been determined by semi-random sampling from their statistical distributions per each section. The term “semi-random” refers to the fact that some limits in the random sampling have been set to avoid sharp geometrical transitions from section to section. In particular, the samples are chosen within a confidence band of 80% (values with a cumulative probability less than  $P=10\%$  and greater than  $P=90\%$  have been discarded). Moreover, samples for adjacent sections are alternately above and below the 50% cumulative probability to reproduce the waviness of the weld toe.<sup>17</sup> This modeling approach was proposed by Lecsek et al.<sup>45</sup> A section width of 1 mm was used in the current study,

which was similar to the proposed width of the evaluation sections for 3D scans (also called slices) by Renken et al.<sup>27</sup>

### 5.1.2 | Modeling of initial defects

The values of the secondary notch depth  $t$  can be determined by a roughness measurement based on ISO 4287:1997 but with some modification according to Zerbst et al.<sup>26</sup> From the large number of roughness parameters defined there, the total height of the roughness profile  $P_t$  is chosen for specifying the secondary notch depth  $t$  near the weld toe. This characterizes the maximum height of the assessed profile. The main difference from the standard is that only a close range next to the weld toe is considered. For test series H to M and O, where no secondary notches could be determined (fillet welds), the initial crack size was determined based on the  $P_t$  value. For butt joints in the current studies, where secondary notches were determined the values of  $t$  were used as initial crack size. The initial crack sizes for each test series are summarized in Table 4.

### 5.1.3 | Cyclic stress–strain behavior

The knowledge of the cyclic stress–strain behavior of the material is of primary importance for the calculation of the elastic–plastic crack driving force.<sup>17</sup> It is assumed that the cyclic stress–strain curve can be represented by the Ramberg–Osgood equation:

$$\varepsilon_a = \frac{\sigma_a}{E} + \left(\frac{\sigma_a}{K'}\right)^{1/n'} \quad (15)$$

In the case of the investigated welded joints, fatigue cracks initiate at the weld toe and the cyclic properties of the HAZ are relevant. For this reason, the parameters  $K'$



**TABLE 4** Parameters of the statistical distribution of the initial defect size (crack depth).

Test series	Initial crack depth $a_i$ (mm)		
	$\hat{E}(X)$ (mm) <sup>a</sup>	$\hat{\sigma}_X$ (mm) <sup>a</sup>	Based on
A1	0.03	0.06	Undercut depth
B1, B2	0.07	0.08	Undercut depth
C1, C2	0.05	0.14	Undercut depth
D1, D2	0.07	0.02	Undercut depth
E1, E2	0.03	0.03	Undercut depth
F1, F2, F3	0.05	0.05	Undercut depth
G1, G2	0.05	0.09	Undercut depth
H1, H2, I1, I2, J1, J2, K1, M1, L1	0.058	0.014	Roughness profile
O1	0.088	0.039	Roughness profile

<sup>a</sup>According to normal distribution.

and  $n'$  have to be determined for the HAZ. This can be done by testing specimens with thermo-physically simulated microstructure<sup>1,46</sup> or by several approximation.<sup>47–49</sup> In this study, the approach according to Lopez and Fatemi<sup>49</sup> based on the Brinell hardness, already proposed by Madia et al.,<sup>17</sup> was used.

#### 5.1.4 | Propagation of short cracks

In a fracture mechanics-based fatigue assessment, it is crucial to consider the fatigue propagation threshold of a growing crack. Usually, in a linear elastic fracture mechanics approach, only the long-crack propagation threshold  $\Delta K_{th,LC}$  is considered. When dealing with the fatigue crack propagation in the physically small crack regime, it must be considered that the fatigue crack propagation threshold  $\Delta K_{th}$  is a function of the crack length due to the development of the crack closure effects. In the current version of the IBESS approach,<sup>17,26</sup> the cyclic  $R$  curve<sup>51</sup> was used to cover the fatigue crack propagation in the physically small crack regime, where a power law function<sup>52</sup> was used for the fit of the threshold  $\Delta K_{th}$ , illustrated in Figure 5B:

$$\Delta K_{th} = \begin{cases} A \cdot \Delta a^b + \Delta K_{th,eff} & \text{for } \Delta a < a_{LC}, \\ \Delta K_{th,LC} & \text{for } \Delta a \geq a_{LC}, \end{cases} \quad (16)$$

where  $A$  and  $b$  are material-dependent parameters and  $\Delta a_{LC}$  is the extension crack length from the physical short- to long-crack regime. The lower bound of this relation is  $\Delta K_{th} = \Delta K_{th,eff}$ , and the values of the intrinsic fatigue crack propagation threshold of  $\Delta K_{th,eff} = 2.7 \text{ MPa mm}^{-1/2}$  were used in this study. According to Zerbst et al.,<sup>26</sup> the microstructure in the

HAZ strongly influences the crack propagation in the physically small crack regime. For this reason, individual values of the material parameters  $A$  and  $b$  were used. The simple method proposed by Zerbst et al.<sup>52</sup> based on the El-Haddad model<sup>53</sup> was used to estimate these parameters depending on the values of  $\Delta K_{th,LC}$ . This method introduces a new parameter,  $a^*$ , which accounts for the fact that  $\Delta K_{th} = \Delta K_{th,eff}$  when  $\Delta a = 0$ :

$$\Delta K_{th} = \Delta K_{th,LC} \cdot \sqrt{\frac{\Delta a + a^*}{\Delta a + a^* + a_0}}. \quad (17)$$

where  $a_0$  is the El-Haddad parameter:

$$a_0 = \frac{1}{\pi} \cdot \left( \frac{\Delta K_{th,LC}}{\Phi \cdot \Delta \sigma_e} \right)^2, \quad (18)$$

in which  $\Delta \sigma_e$  is the fatigue limit range for smooth specimen. The fatigue limit range is estimated based on the material's strength or hardness (see Section 5.1.6). A shape factor of  $\Phi = 0.728$  was used.<sup>54</sup> The additional parameter in Equation (17) can be determined for  $\Delta K_{th} = \Delta K_{th,eff}$  at  $\Delta a = 0$  by the following equation:

$$a^* = a_0 \cdot \frac{\left( \frac{\Delta K_{th,eff}}{\Delta K_{th,LC}} \right)^2}{1 - \left( \frac{\Delta K_{th,eff}}{\Delta K_{th,LC}} \right)^2}. \quad (19)$$

The model was applied for a different stress ratio according to Zerbst et al.<sup>26</sup> (see Section 5.1.6). Finally,  $A$  and  $b$  were determined by least squares fitting of Equations (16) and (17).

For the sake of understanding the results of the fatigue assessment, it is important to mention that the

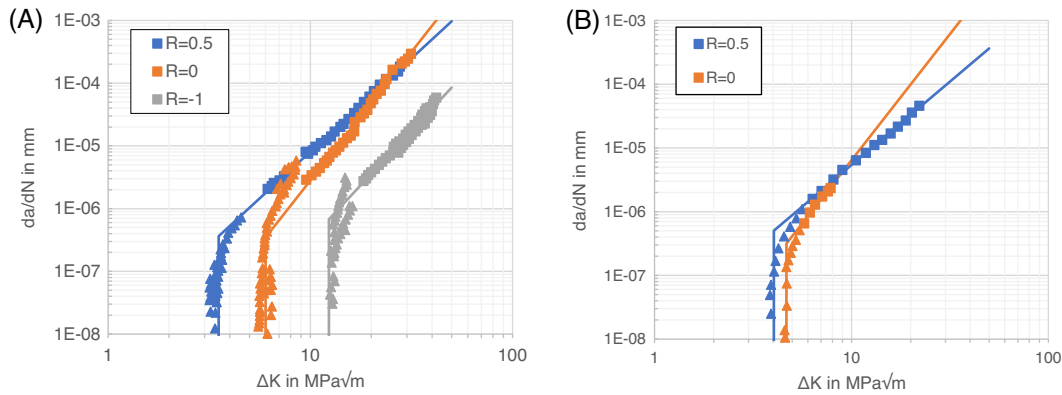


**FIGURE 6** Crack propagation curve for steel (A) S355 and (B) S960 for different stress ratios. [Colour figure can be viewed at [wileyonlinelibrary.com](http://wileyonlinelibrary.com)]

approximation of the fatigue crack growth resistance in the short-crack regime (cyclic  $R$  curve) given by the modified El-Haddad model tends to overestimate the experimental values. This leads to the important conclusion that the effective crack driving force ( $\Delta K_{eff}$ ) is underestimated and therefore the fatigue strength overestimated.

### 5.1.5 | Propagation of long cracks

The fatigue crack propagation in the physically long-crack regime in the IBESS procedure, illustrated in Figure 5C, is described by the following equation:

$$\frac{da}{dN} = C \cdot (\Delta K_{eff})^m \cdot \left(1 - \frac{\Delta K_{th}(a)}{\Delta K}\right)^p, \quad (20)$$

where  $\Delta K_{eff}$  is the effective stress intensity factor (SIF) range including the crack closure factor  $U(a)$  (with  $\Delta K_{eff} = \Delta K U(a)$ ). The parameter  $p$  is used for fitting experimental data to the crack threshold regime and is set to  $p = 0.8$  for all calculations in this study.

To determine the parameters of the physically long-crack regime, the database of the IBESS cluster was used for the base material of S355NL and S960 for different stress ratios (see Figure 6). The values for  $C$  and  $m$  are calculated according to ASTM E647<sup>55</sup> and documented in Table 5. The SIF in this study was calculated according to the solution of Wang and Lambert<sup>56</sup> (i.e., a weight function approach for semi-elliptical surface cracks).

### 5.1.6 | Fatigue limit

In the IBESS procedure, the determination of the endurance or fatigue limit of the material is essential to the calculation of the critical initial crack size in cases of

flawless materials.<sup>17</sup> The fatigue limit needs either to be determined by experiments or estimated by the following relation:

$$\sigma_e \approx 0.45 R_m \approx 1.6 \text{ HV for } R = -1 \text{ with } \sigma_e = \Delta\sigma_e/2, \quad (21)$$

being valid for a limited range of  $R_m \leq 1400$  MPa and HV  $\leq 400$  according to the FKM guideline,<sup>7</sup> where  $R_m$  is the material's tensile strength and HV is the Vickers hardness. With respect to the fatigue limit range  $\Delta\sigma_e$  (see Equation 18), a conversion to a different stress ratio  $R$  must be carried out such as is usual in fatigue calculations. An option is provided by the Haigh approach, for example, using Goodman's equation:

$$\sigma_\alpha(R) = \frac{\sigma_e(R = -1)}{\left(1 + \frac{\gamma(R) \cdot \sigma_e(R = -1)}{R_m}\right)}, \quad (22)$$

with  $\gamma(R)$  being a conversion factor, which can simply be determined as

$$\gamma = \frac{\sigma_m}{\sigma_\alpha} = \frac{1+R}{1-R}. \quad (23)$$

In this study, the conversion factors  $\gamma = 0$  for  $R = -1$ ,  $\gamma = 1$  for  $R = 0$  and  $R = 0.1$ , and  $\gamma = 3$  for  $R = 0.5$  were used according to Zerbst et al.<sup>26</sup> In line with the presented approach for the estimation of the parameters  $A$  and  $b$  (see Equations 16 to 19), the effect of different stress ratios  $R$  and mean stress is considered.

### 5.1.7 | Consideration of welding residual stresses

The consideration of welding residual stresses in the IBESS approach was proposed by Hensel et al.<sup>2</sup> and

TABLE 5 Input parameters for the IBESS approach.

Test series	Cyclic $\sigma$ - $\epsilon$ curve		Parameter for cyclic R curve			Paris law constants	
	$K'$ (MPa)	$n'$ (MPa)	$\Delta K_{th,LC}$ (MPa m <sup>1/2</sup> )	$A$ (-)	$b$ (-)	$\log_{10}(C)$ (MPa m <sup>1/2</sup> )	$m$ (-)
A1 <sup>a</sup>	1184	0.212	6.00	3.260	0.321	-8.010	2.71
B1	1557	0.173	3.52	0.685	0.321	-8.066	2.97
B2			6.00	3.260	0.320		
C1	1355	0.192	12.36	9.012	0.299		
C2	1355	0.192	6.00	2.406	0.395		
D1	1305	0.198	6.00	2.871	0.313		
D2			3.52	0.603	0.398		
E1	1378	0.190	3.52	0.633	0.371		
E2			6.00	3.079	0.322		
F1	1538	0.174	3.52	0.681	0.326		
F2			6.00	3.557	0.341		
F3			12.36	9.012	0.299		
G1 <sup>a</sup>	1541	0.175	8.30	6.424	0.332	-8.106	2.93
G2 <sup>a</sup>			5.40	5.672	0.202		
H1, I1	1433	0.048	4.67	3.237	0.328	-7.883	2.61
H2, I2			4.07	1.731	0.360		
J1	1119	0.109	6.00	4.137	0.347	-8.066	2.97
J2			3.52	0.776	0.335		
K1	1643	0.165	6.00	3.812	0.341		
K2			3.52	0.722	0.324	-8.066	2.97
L1	1433	0.048	4.67	3.237	0.328	-7.883	2.61
M1	1119	0.109	6.00	4.137	0.347	-8.066	2.97
N1	1432	0.184	6.00	3.238	0.329		
O1	1507	0.177	6.00	3.448	0.335		

<sup>a</sup>Estimated from the FKM guideline.<sup>50</sup>

described by Zerbst et al.<sup>26</sup> In general, residual stresses can be considered as additional mean stresses if they are stable over a large portion of the lifetime. However, detailed knowledge about the residual stress distribution through thickness is necessary as well as knowledge about the behavior of the residual stress under cyclic loading. In nearly all the welded joints investigated, this information was not available. Residual stress measurements by X-ray diffraction of test series H to M<sup>35</sup> and N<sup>36</sup> in as-welded conditions showed a low residual stress level at the surface of the weld toe. However, numerical assessment of the residual stresses by structural welding simulation of welded joints H to M<sup>33</sup> showed a higher tensile residual stress level below the surface layer. Because of the mentioned uncertainties, welding residual stresses are not considered in the current study.

### 5.1.8 | Simulation algorithm

According to the IBESS approach, fatigue tests under constant loading were simulated for different load levels taken from the experimental  $S$ - $N$  curves (see Figure 7). Geometrical parameters were taken into account through statistical distribution of the weld geometry (see Sections 5.1.1 and 5.1.2). Fatigue crack growth was calculated for the physically short- and long-crack regime (see Sections 5.1.4 and 5.1.5), under consideration of crack coalescence. The best way of carrying out a full probabilistic fatigue assessment considering the statistical distributions of geometrical and material parameters is to adopt a simulation technique similar to the Monte Carlo method. This is implemented in the IBESS procedure, whereby a new weld toe geometry is generated by random sampling for each simulation. Due to the high

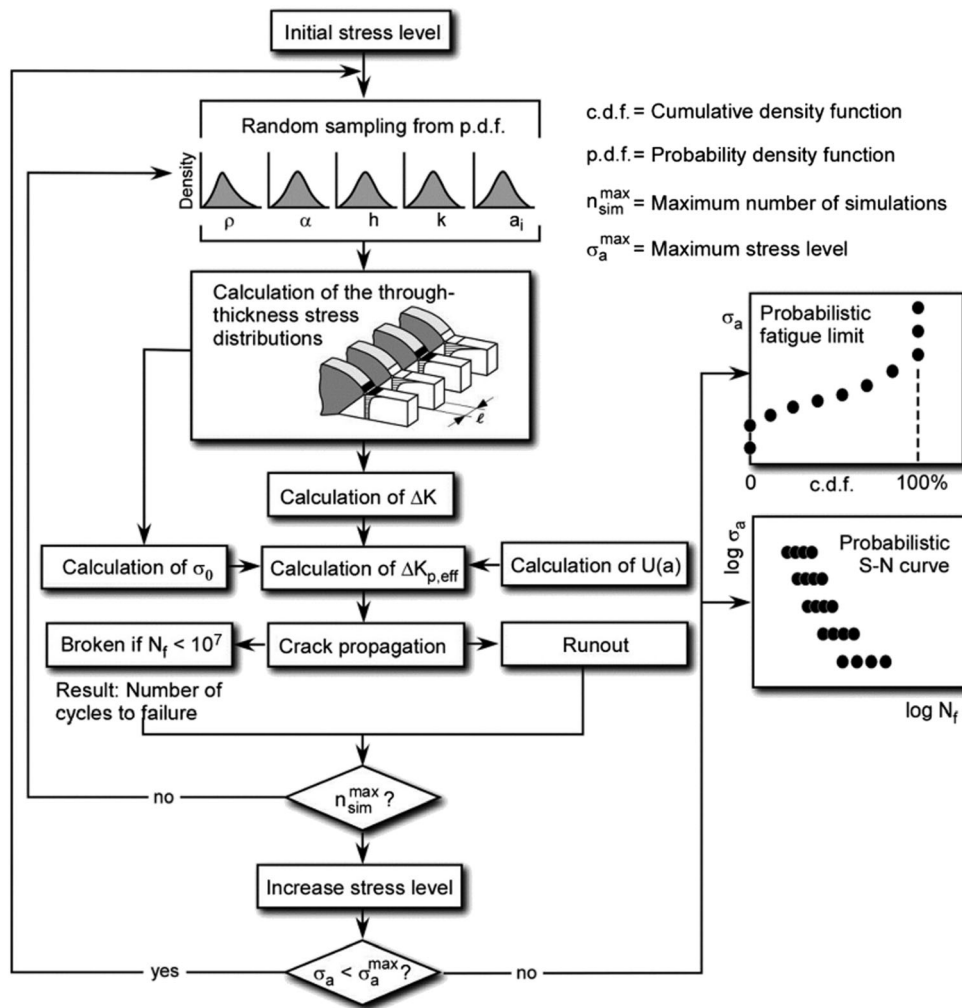


FIGURE 7 Flow chart of the computational algorithm of the IBESS approach.<sup>17</sup>

computational effort required, 20 simulated fatigue test results were calculated. This number ensures a lower rate of statistical error compared to the evaluation of the experimental tests. The fatigue test results are uniformly distributed over at least five load levels. A minimum ratio between the highest and lowest load level of a fatigue test series of at least 1.2 according to Haibach<sup>57</sup> was used. After the simulated fatigue test had been calculated, the same statistical evolution was performed for the experimental fatigue test results (see Section 4).

## 5.2 | Comparison with experimental data

A comparison between the experimentally determined  $S-N$  curves and  $S-N$  curves calculated by the IBESS approach was performed. For this, the characteristic values of fatigue strength  $\Delta S_{50\%}$  (nominal stress range at  $2 \times 10^6$  load cycles and  $P_f = 50\%$ ), fatigue strength  $\Delta S_{2.5\%}$  (nominal stress range at  $2 \times 10^6$  load cycles and  $P_f = 2.5\%$ ), inverse slope  $k$ , and scatter range  $T_N$  (see

Section 4) were compared based on the experimental results (Exp) and the results calculated by the IBESS approach. The comparison is illustrated in Figure 8A–D. As shown, the IBESS approach ranges from an underestimation of  $\Delta S_{50\%}$  of  $-18\%$  (test series O1) to an overestimation of  $180\%$  (test series C1) (see Figure 8A). Good agreement (with a difference of less than 30%) was determined for test series B1, B2, C2, D2, F1, F2, G1, H1, H2, I1, I2, J1, J2, K1, K2, N1, and O1, which represent around 70% of the experimental data. For all test series with  $R = 0.5$  and for all test series of cruciform joints and T-joints, good correlation was determined between experimental values and the values calculated by the IBESS approach. Very high disagreement was determined for test series C1 and F3 tested at  $R = -1$ .  $\Delta S_{2.5\%}$  was overestimated by the IBESS approach compared with experimental values (see Figure 8B). This is related to the underestimation of the scatter range  $T_N$ , shown in Figure 8C. Only for test series B1, B2, D1, D2, F1, K1, M1, N1, J1, and O1 was a good correlation determined (with a difference of less than 30%). These experimental test series show a comparably low scatter range of  $T_N < 2.1$ . In general, all values of  $T_N$

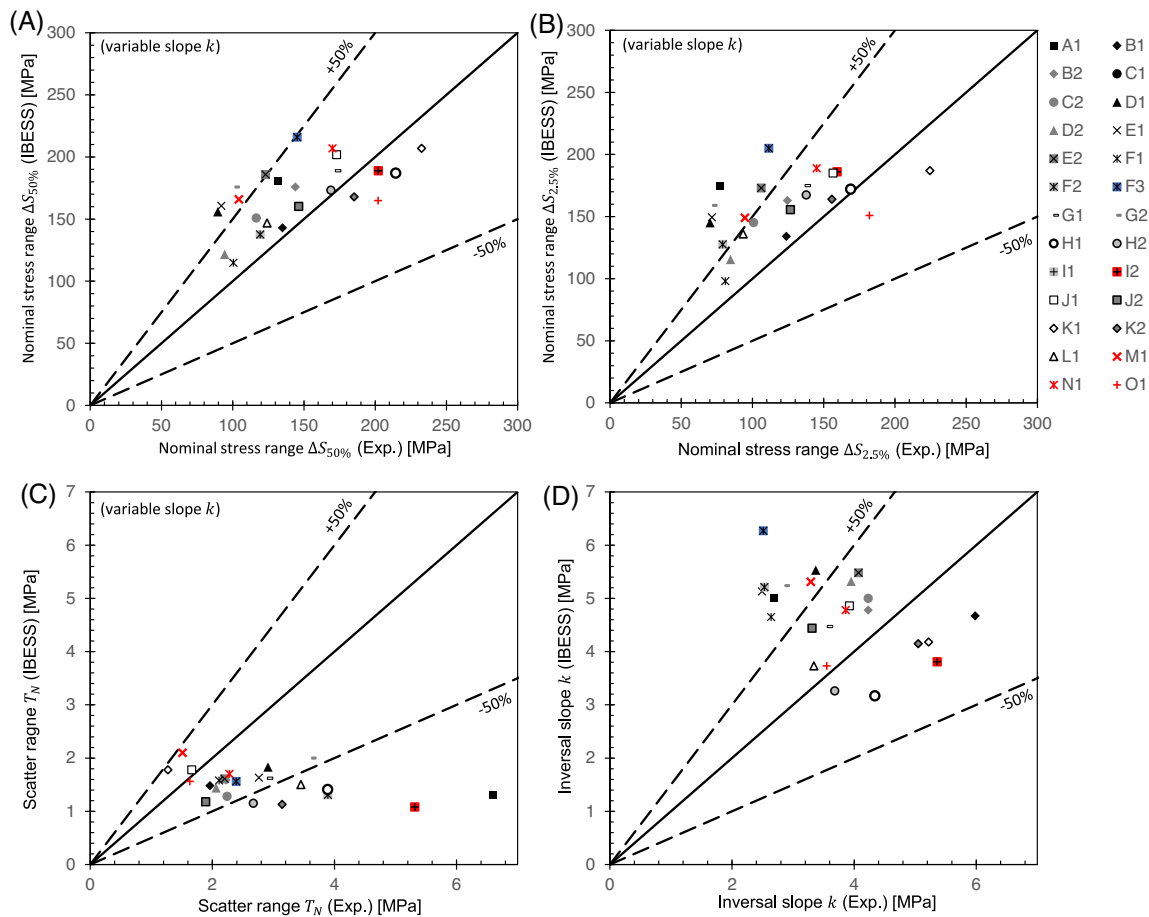


**FIGURE 8** Correlation of experimental vs. calculated (IBESS) values of (A)  $\Delta S_{50\%}$ , (B)  $\Delta S_{97.5\%}$ , (C)  $T_N$ , and (D)  $k$ . [Colour figure can be viewed at [wileyonlinelibrary.com](https://onlinelibrary.wiley.com)]

calculated by the IBESS approach were lower than 1.7, while values of  $T_N$  determined from the experimental values range from 1.63 to 6.59. Regarding the evaluated inverse slope  $k$ , good agreement was determined for most of the calculated test series. Only test series A1, D1, E1, F1, F2, G2, and O1 show higher deviation of more than 30%. For nearly all test series with a high agreement of  $k$ , a high agreement of  $\Delta S_{50\%}$  was also determined.

## 6 | LOCAL WELD GEOMETRY VERSUS FATIGUE STRENGTH

As mentioned, it is trivial that the local geometry at the weld toe strongly affects the local stress concentration and the fatigue strength of the welded joint. The relation between the single geometrical parameter ( $\rho, \alpha, t$ , and  $h$ ) and the fatigue strength is investigated by Schork et al.<sup>16</sup> for theoretical values of  $\rho, \alpha, t$ , and  $h$ . In this study, however, the investigations were performed using real values for the geometrical parameters and fatigue strength (see Tables 3 and 5). The results are displayed in Figure 9.

Values of  $\Delta S_{2.5\%}$  evaluated with a fixed slope of  $k=3$  according to the IIW recommendation<sup>4</sup> are used. For comparison with the IIW FAT classes, the evaluated fatigue strength  $\Delta S_{2.5\%}$  ( $k=3$ ) was corrected by the enhancement factor  $f(R)$ , proposed by the IIW recommendation,<sup>4</sup> with  $\Delta S_{2.5\%}(k=3)/f(R)$  for  $-1 > R > 0.5$ . For test series H to M, low residual stresses  $\sigma_{res}$  at the weld toe were determined ( $\sigma_{res} < 0.2\sigma_Y$ , where  $\sigma_Y$  is the yield strength of the base material), the enhancement factor were determined with  $f(R) = -0.4R - 1.2$ . For all other test series, a medium residual stress level was assumed, with  $f(R) = -0.4R - 0.9$ . The corrected values of  $\Delta S_{2.5\%}$  ( $k=3$ ) were plotted against the mean values of the geometrical parameter weld toe radius  $\rho_{50}$ , weld toe angle  $\alpha_{50}$ , and secondary notch depth  $t_{50}$  (if  $t$  could be determined from 3D scans) (see Figure 9). Furthermore, the values of  $\rho_{10}$ ,  $\alpha_{90}$ , and  $t_{90}$  were plotted, which belong to a cumulative probability of  $P=10\%$  or  $P=90\%$  based on the used normal distribution or log-normal distribution. The values were calculated according to Equations (1) and (2) (e.g., with  $P(x) = 0.1$  for  $\rho_{10}$ ). This accounts for the fact



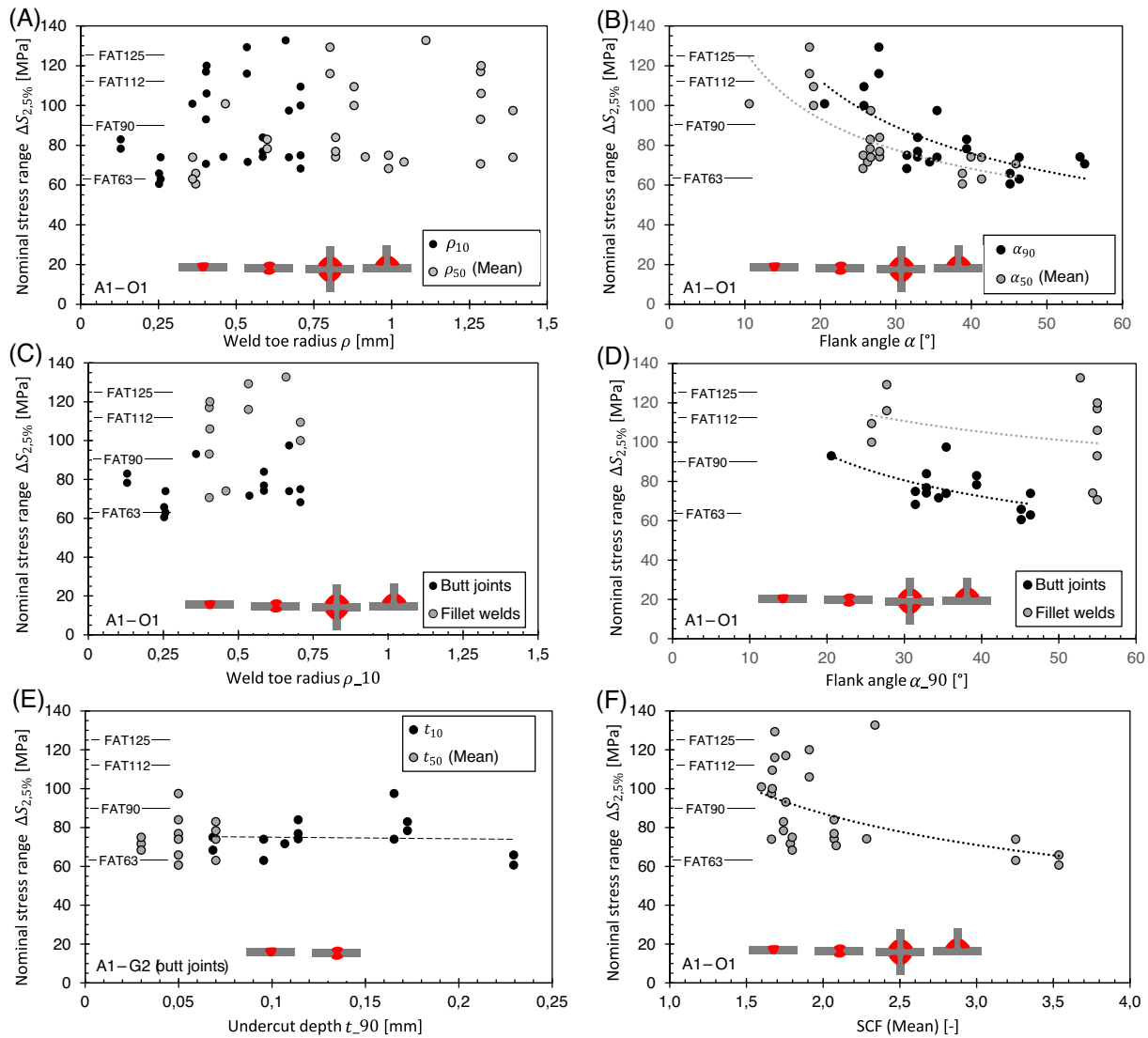


**FIGURE 9** Correlation of experimentally determined fatigue strength with different geometrical parameters: (A) flank angle and (B) weld toe radius for all test series (A1 to O1), (C) flank angle and (D) weld toe radius for the test series with  $R = 0.5$ , and (E) the undercut depth and (F) the mean SCF. [Colour figure can be viewed at [wileyonlinelibrary.com](https://onlinelibrary.wiley.com)]

that fatigue cracks start from locations with high stress concentrations, and it is assumed that mean values of geometrical parameters do not represent locations with high stress concentrations. Note that the values of  $\rho_{10}$  are lower than the mean value  $\rho_{50}$ . While the values  $\alpha_{90}$  and  $t_{90}$  are higher than the mean value  $\alpha_{50}$  and  $t_{50}$  because a higher flank angle and secondary notch depth lead to an increase in the SCF, lower values of the weld toe radius lead to an increase in the SCF as well.

While Figure 9A shows a high scatter of the weld toe radius with nearly no correlation to the fatigue strength, an increase in the fatigue strength  $\Delta S_{2.5\%}$  is shown for increasing values of the flank angle (see Figure 9B). Regarding the relation of  $\alpha_{90} \sim \Delta S_{2.5\%}$  for butt joints and fillet welds (see Figure 9D), an increasing trend was observed. For butt joints with a comparably low flank

angle  $\alpha_{90} \approx 20^\circ$ , the trend line is close to the class FAT 90, while a value of  $\alpha_{90} \approx 45^\circ$  is close to FAT 71. For the secondary notch depth  $t$ , no increasing trend was determined (see Figure 9E). Additionally, the SCF was also plotted against  $\Delta S_{2.5\%}$  (see Figure 9F). The solution according to Kiyak et al.<sup>29</sup> was used for the calculation of SCF with the mean values of  $\rho$  and  $\alpha$ . As shown, a decreasing trend of  $\Delta S_{2.5\%}$  with increasing SCF was observed over all test series. Following the trend line, a value of  $SCF \approx 1.6$  in mean falls in the range of FAT 100, while a value of  $SCF \approx 3.6$  corresponds with the FAT 63. However, in general, it is clearly shown that a high scatter in the data, especially for the weld toe radius and secondary notch depth, makes interpretations very difficult. Lower scatter is observed in the flank angle and SCF.

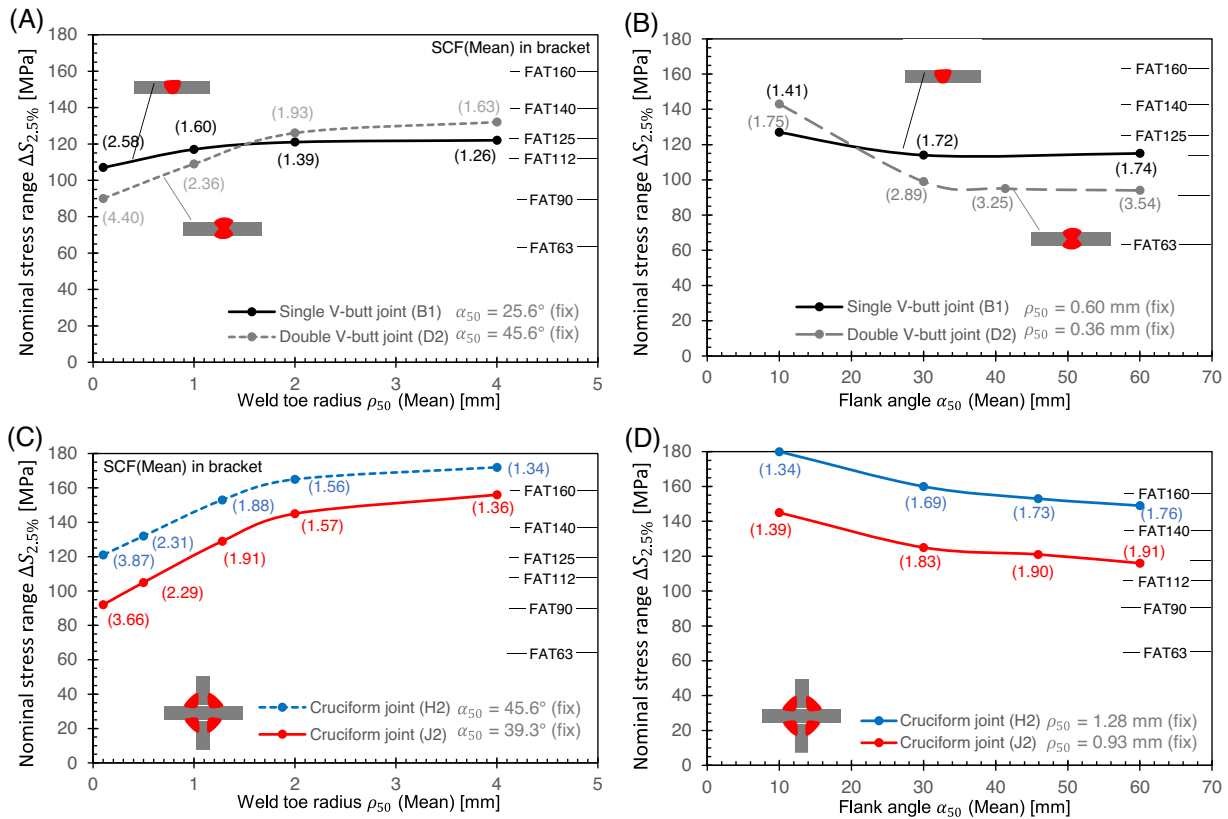


FIGURE 10 Nominal stress range  $\Delta S_{2.5\%}$  (for  $k=3$ ) under variation of (A,C) weld toe radius (mean) and (B,D) flank angle (mean) calculated by the IBESS approach. [Colour figure can be viewed at [wileyonlinelibrary.com](http://wileyonlinelibrary.com)]

For further investigations regarding the correlation of geometrical parameters and fatigue strength, the IBESS approach was used, as plotted in Figure 10. The mean SCF was also calculated and displayed in brackets in the same graph. Calculations were made with the data of four test series (B1, D2, J2, and H2) that show less deviation with experimentally determined values of  $\Delta S_{2.5\%}$ ,  $\Delta S_{50\%}$ , and  $T_N$  (see Section 5.2). All test series were tested with a stress ratio of  $R=0.5$ . Calculations were made using the IBESS approach by varying the mean value of weld toe radius  $\rho$  and flank angle  $\alpha$ . All other parameters were constant. The weld toe radius was varied over the complete range of the used SCF solution<sup>29</sup> from  $0.01 < \rho/T < 0.4$ , and the weld flank angle was varied in the range of  $10^\circ < \alpha < 60^\circ$ .

A decrease in the weld toe radius leads to a lower increase of  $\Delta S_{2.5\%}$  for test series B1 (single V-butt joint) compared with test series D2 (double V-butt joint) (see Figure 10A). For low values of  $\rho$ ,  $\Delta S_{2.5\%}$  is close to FAT100 for B1 and FAT90 for D2. The stronger increase of  $\Delta S_{2.5\%}$  correlates also with the higher SCF for D2 compared with B1. Similar results are displayed in Figure 10B for test series B1 and D2 under variation of  $\alpha_{50}$  when  $\rho_{50}$  was constant. Again, in this case, the change of  $\Delta S_{2.5\%}$  is higher for D2 than for B1, which correlates with the

higher change in the SCF. For high values of  $\alpha_{50}$  of  $60^\circ$ , the  $\Delta S_{2.5\%}$  is close to FAT112 for B1 and FAT90 for D2. For the two cruciform joints test series J2 and H2, the calculations are displayed in Figure 10C and Figure 10D. It is shown that the curves of  $\Delta S_{2.5\%}$  are mostly parallel for both test series, corresponding to the similar SCF for both cases. The changes of  $\Delta S_{2.5\%}$  are related to the different material properties for J2 (S355J2+N) and H2 (S960QL). Similar to the calculations of test series B1 and D2, a variation in the weld toe radius seems to have a higher influence on  $\Delta S_{2.5\%}$  than a variation in the weld flank angle. Furthermore, throughout the four tests series B1, D2, J2, and H2, it is shown that for a mean weld toe radius of  $\rho_{50} > 2$  mm no significant change of  $\Delta S_{2.5\%}$  was determined. For the mean flank angle, the larger deviation was determined for  $\alpha_{50} < 30^\circ$ .

## 7 | DISCUSSION

Fatigue tests were simulated using the IBESS approach for 26 different test series covering four different weld details, different base materials, different weld geometry, and different load types and stress ratios  $R$ . The best agreement was reached for the simulations with  $R=0.5$ ,

whereas the worst results were obtained for  $R = -1$ . It is assumed that this is related to the assumptions made for some important input parameters, particularly the cyclic  $R$  curve, as mentioned in Section 5.1.4. The authors suspect that the higher crack propagation resistance associated to the El-Haddad model and therefore the lower effective crack driving force are the most reasonable explanation for the overestimation of the fatigue strength. This would explain the good results obtained for the higher stress ratios, where the closure effects are vanishingly small. A further reason could reside in the omission of residual stresses for the IBESS simulations in this study (see Section 5.1.6). In some of the test series (H to N), a low residual stress level (at least at the surface) was determined; for these test series, good agreement was also determined for lower load ratios of  $R = 0.1$ . In combination, the need for accurate residual through-thickness stress profiles and the behavior of the residual stresses under cyclic loading for every specimen require a high experimental effort.<sup>26</sup> However, for a practical consideration of welding residual stresses in this approach, a mean stress correction proposed by Hensel et al.<sup>58</sup> and Hensel<sup>59</sup> may be possible and should be considered for further investigations.

In general, it is shown that the assumptions made in this study lead to the overestimation of the fatigue life and fatigue strength of welded joints. Furthermore, there are intrinsic modeling assumptions in the IBESS procedure that should be discussed. First, it should be mentioned that the IBESS approach was developed for butt joints, including the used solution for the calculation of the SCF and through-thickness stress distribution<sup>29</sup> and the used solution for the SIF.<sup>56</sup> Regarding the SCF solution, however, it was already successfully applied for cruciform joints as well by Madia et al.<sup>17</sup> Regarding the SIF solution, however, it is assumed that the solution for semi-elliptic cracks in flat plates is satisfying the condition for butt joints with a comparably low weld height. For T-joints or cruciform joints, the stiffness is obviously higher, and the solution may underestimate the SIF factor. This may explain the trend toward non-conservative results. Thus, the IBESS simulation of test series H to M and O (cruciform joints and T-joints) showed good agreement with the experimental results. However, it could not exclude that a systematic underestimation of the geometrical parameter from the 3D scans (especially the weld toe radius  $\rho$ ) is also responsible for the non-conservative trend in IBESS simulations.

For nearly every simulated test series with the IBESS approach, an underestimation of the scatter range  $T_N$  was observed. It can be assumed that this is related to the input data, especially to the scatter of the geometrical parameter weld toe radius  $\rho$ , flank angle  $\alpha$ , secondary

notch depth  $t$ , or the initial crack depth  $a_i$ . Comparison between simulated fatigue tests using the IBESS approach and experimental fatigue tests showed that the simulated results produced a lower scatter than the experimental results.<sup>17</sup> The limited resolution of the measurement system may lead to an overestimation of the evaluated parameter and to non-conservative results regarding the simulated fatigue tests, especially if the geometrical features are small like the weld toe radius and the secondary notch depth, as mentioned already by Schubnell et al.<sup>20</sup> and Braun et al.<sup>28</sup> Another factor that leads to an underestimation of the scatter in the used approach is the differences in the theoretical statistical distributions that tend to eliminate outliers. Braun et al.<sup>28</sup> already mentioned that the used statistical distributions are not able in every case to describe the real distributions with an acceptable accuracy. Furthermore, the scatter of the material properties has not been considered, which could have a remarkable influence on the scatter of the predictions, especially considering the scatter in the crack propagation data. Last but not least, the misalignment and the angular distortion were not considered in the calculations.

Regarding the numerically calculated correlation between geometrical parameters and the evaluated fatigue strength (see Figure 10), it is clearly shown that a change in the weld toe radius  $\rho$  has a higher influence on the fatigue strength in the simulations than the flank angle  $\alpha$ . Schork et al.<sup>16</sup> showed that the influence of the weld toe radius  $\rho$  depends especially on the depth of the secondary notch.

However, in the mentioned study, it is also shown that for a low secondary notch depth, no significant influence on the fatigue strength of welded joints was determined if the weld toe radius  $\rho > 2$  mm, similar to the results of this study. It is also shown that the majority of the determined weld toe radii are below a value of  $\rho < 2$ , with mean values of  $\rho = 0.86$  mm over test series A to O. Thus, it is questionable if a weld toe radius of  $\rho \geq 4$  mm is really applicable in the ISO 5817:2014<sup>22</sup> and the STD 181-0004<sup>24</sup> standards. Regarding the flank angle  $\alpha$ , however, a value of  $\alpha \leq 30^\circ$  (for butt joints) for the highest quality class B125 in ISO 5817:2014 seems meaningful according to the results of this study, because above these values, a stronger decrease in the fatigue strength was observed.

According to the authors, the IBESS approach<sup>17,26</sup> combined with previous work<sup>20,27</sup> regarding the evaluation of geometrical parameter and statistical evaluation<sup>28</sup> is a good method for the fatigue assessment of welding joints based on their individual geometry and material properties and can help to decrease the strong conservatism regarding the fatigue design of welded joints and

components by using individual geometry and material properties. However, this approach needs a large number of input parameters: geometrical parameters ( $\rho, \alpha, t$ ) and their statistical distributions, material constants for short-crack ( $A, b, \Delta K_{th,eff}$ ) and long-crack propagation models ( $C, m, \Delta K_{LC}$ ) and cyclic stress strain behavior ( $K', n', E$ ), and fatigue limit ( $\sigma_e$ ). Thus, some parameters could easily be approximated ( $A, b, \Delta K_{th,eff}, K', n', E$ ) according to Zerbst et al.<sup>52</sup> and Lopez and Fatemi,<sup>49</sup> or taken from guidelines ( $C, m, \Delta K_{LC}, \sigma_e$ ) like the FKM<sup>50</sup> or IIW guidelines.<sup>4</sup> Nevertheless, the approximations must be checked carefully, as it is demonstrated in this study that some modeling assumptions could lead to non-conservative predictions of the fatigue strength. The highest effort is needed for the determination of the geometrical parameters ( $\rho, \alpha, t$ ). No standardized method exists currently for their determination. It is recommended that further attention should be paid regarding this issue.

## 8 | CONCLUSIONS

A method is proposed and tested in this study for the probabilistic fatigue assessment of welded joints based on their individual geometrical parameters using a combination of methods from previous studies.<sup>17,20,27,28</sup> The geometrical parameters were evaluated from 3D surface scans of 26 test series from previous studies<sup>30–36</sup> of welded joints.

The study focused on a comprehensive comparison between the experimental results and the calculated results of the IBESS approach. For this comparison, the characteristics of the  $S-N$  curve  $\Delta S_{2.5\%}$ ,  $\Delta S_{50\%}$  (nominal stress range  $\Delta S$  at  $2 \times 10^6$  load cycles and a failure probability of  $P_f = 50\%$ ), scatter range  $T_N$ , and slope  $k$  were compared. The following conclusions can be drawn:

- Given the assumptions made in this investigation, the IBESS approach tended to overestimate the fatigue strength  $\Delta S_{2.5\%}$  of welded joints for load ratios  $R < 0.5$ . For  $R = 0.5$ , good agreement with experimental values was determined for all types of the investigated welded joints (butt joints as well as cruciform and T-joints). The use of a simplified model for the description of the fatigue crack growth resistance is the explanation for the non-conservative results.
- The calculated slope  $k$  was in good agreement with the experimental determined slope. For 18 out of 26 calculations the slope was within a range of  $\pm 50\%$  compared with the slope evaluated from experimental fatigue test. The non-consideration of residual stresses may also explain some differences, as well as differences in the material properties ( $C, m, \Delta K_{LC}, \sigma_e$ ).

- The scatter range  $T_N$  was underestimated for every calculated test series in this study. This underestimation is directly related to an overestimation of  $\Delta S_{2.5\%}$ . However, for some test series with a comparable low scatter range of  $T_N > 2$ , good agreement with experimental values was reached. Furthermore, it should be mentioned that the underestimation of the scatter in the simulated fatigue test could also be related to an underestimation of the scatter of the geometrical parameters and the initial crack depth.

The empirical correlation between the geometrical parameters and the fatigue strength was also investigated in this study, and the following conclusions can be drawn:

- No strong correlation of the weld toe radius with the fatigue strength ( $\rho \sim \Delta S_{2.5\%}$ ) was determined. Therefore, it is not clear if this scatter regarding the weld toe radius  $\rho$  is reflected in the scatter of the fatigue lives. Issues related to the different measurement systems and parameters used make the interpretation of the results difficult.
- Regarding the correlation of flank angle and fatigue strength ( $\alpha \sim \Delta S_{2.5\%}$ ), a clear trend was observed. For butt joints, a flank angle of  $\alpha \approx 20^\circ$  correlates with the fatigue class FAT90 while a flank angle of  $\alpha \approx 45^\circ$  correlates with FAT71.
- No increasing trend was observed for the correlation of the secondary notch or undercut depth  $t$  with the fatigue strength. However, it is assumed that this is related to the fact that the used theoretical normal distributions do not represent the real (skewed) distribution (see Braun et al.<sup>28</sup>). Furthermore, it should be mentioned that according to previous work,<sup>16</sup> a higher influence of  $t$  than of  $\rho$  and  $\alpha$  was strongly assumed. However, the evaluation of  $t$  from 3D scans is perhaps related to a higher error because this geometrical feature is comparably small to typical scanning resolutions.

Further calculations using the IBESS approach with different weld toe radius  $\rho$  and flank angle  $\alpha$  showed that the evaluated fatigue strength  $\Delta S_{2.5\%}$  does not significantly change for values  $\rho > 2$  mm and for values  $\alpha < 30^\circ$ . The influence of  $\rho$  seems much higher than the influence of  $\alpha$ , similar to the results of previous investigations.<sup>16</sup>

In summary, this study poses the problem of the quality of the input data for modeling the fatigue life of weldments. In fact, a fracture mechanics model such as the IBESS procedure which encloses the most relevant modeling aspects and considers the local weld geometry can overestimate the fatigue life and fatigue strength of



welded joints in some cases. The main reason is attributed to an overestimation of the crack propagation threshold in the short-crack regime which is a crucial material input for the correct estimation of the effective crack driving force. It is recommended that further investigations focus on this issue. Also, global distortions and misalignment should be considered in the future in this approach for the fatigue design of larger components and assemblies. Furthermore, it should be mentioned that developing a standardized procedure for the evaluation of geometrical parameters of welded joints may be an important factor in further generation of a database of these parameters to be used in fatigue assessments by this probabilistic method.

## AUTHOR CONTRIBUTIONS

*Draft preparation:* Jan Schubnell. *Calculations and data arrangement:* Jan Schubnell and Sai Kumar Konidena. *Statistical analysis:* Matthias Jung. *Data provision:* Jan Schubnell, Moritz Braun, and Daniel Löschner. *Writing, reviewing, and editing:* Mauro Madia, Moritz Braun, Matthias Jung, Sören Ehlers, and Thomas Kannengießer. All authors have read and agreed to the published version of the manuscript.

## CONFLICT OF INTEREST STATEMENT

The authors declare that there are no conflicts of interest.

## ACKNOWLEDGEMENTS

Open Access funding enabled and organized by Projekt DEAL.

## DATA AVAILABILITY STATEMENT

Research data are not shared.

## ORCID

Moritz Braun  <https://orcid.org/0000-0001-9266-1698>

## REFERENCES

- Kucharczyk P, Madia M, Zerbst U, Schork B, Gerwien P, Münstermann S. Fracture-mechanics based prediction of the fatigue strength of weldments. Material aspects. *Eng Fract Mech.* 2018;198:79-102. doi:10.1016/j.engfracmech.2017.09.010
- Hensel J, Nitschke-Pagel T, Tchoffo Ngoula D, Beier H-T, Tchuindjang D, Zerbst U. Welding residual stresses as needed for the prediction of fatigue crack propagation and fatigue strength. *Eng Fract Mech.* 2018;198:123-141. doi:10.1016/J.ENGFRACMECH.2017.10.024
- Schork B, Kucharczyk P, Madia M, et al. The effect of the local and global weld geometry as well as material defects on crack initiation and fatigue strength. *Eng Fract Mech.* 2017;198:103-122. doi:10.1016/j.engfracmech.2017.07.001
- Hobbacher AF. *Recommendations for Fatigue Design of Welded Joints and Components*. 2nd ed. Springer; 2016.
- European Committee for Standardization. *Eurocode 3: Design of steel structures—Part 1-9: Fatigue, 1993-1-9:2005*. European Committee of Standardization; 2009.
- BSI. BS 7608, Code of practice for fatigue design and assessment of steel structures. 1993.
- Rennert R, Kullig E, Vormwald M, Esderts A, Siegele D. *FKM-Richtlinie: Rechnerischer Festigkeitsnachweis für Maschinenbauteile*. 6th ed. VDMA Verlag; 2012.
- Lieurade HP, Huther I, Lefebvre F. Effect of weld quality and postweld improvement techniques on the fatigue resistance of extra high strength steels. *Weld World.* 2008;52(7-8):106-115.
- Ning Nguyen T, Wahab MA. A theoretical study of the effect of geometry parameters on the fatigue crack propagation life. *Eng Fracture Mech.* 1995;51(1):1-18.
- Barsoum Z, Jonsson B. Fatigue assessment and LEM analysis of cruciform joints fabricated with different welding processes. *Weld World* 2008. 2013;52(7):93-105. doi:10.1007/BF03266657
- Jonsson B, Samuelsson J, Marquis GB. Development of weld quality criteria based on fatigue performance. *Weld World.* 2011;55(11-12):79-88. doi:10.1007/BF03321545
- Nykänen T, Marquis GB, Björk T. A simplified fatigue assessment method for high quality welded cruciform joints. *Int J Fatigue.* 2009;31(1):79-87.
- Barsoum Z, Jonsson B. Influence of weld quality on the fatigue strength in seam welds. *Eng Fail Anal.* 2011;18(3):971-979. doi:10.1016/J.ENGFAILANAL.2010.12.001
- Lindgren E, Stenberg T. *Quality Inspection and Fatigue Assessment of Welded Structures*. KTH Stockholm; 2011.
- Åstrand E, Stenberg T, Jonsson B, Barsoum Z. Welding procedures for fatigue life improvement of the weld toe. *Weld World.* 2016;60(3):573-580. doi:10.1007/s40194-016-0309-9
- Schork B, Zerbst U, Kiyak Y, Kaffenberger M, Madia M, Oechsner M. Effect of the parameters of weld toe geometry on the FAT class as obtained by means of fracture mechanics-based simulations. *Weld World.* 2020;64(6):925-936. doi:10.1007/S40194-020-00874-7/FIGURES/14
- Madia M, Zerbst U, Beier HT, Schork B. The IBESS model—elements, realisation and validation. *Eng Fract Mech.* 2018;198:171-208. doi:10.1016/j.engfracmech.2017.08.033
- Hultgren G, Barsoum Z. Fatigue assessment in welded joints based on geometrical variations measured by laser scanning. *Weld World.* 2020;64(11):1825-1831. doi:10.1007/s40194-020-00962-8
- Hultgren G, Myrén L, Barsoum Z, Mansour R. Digital scanning of welds and influence of sampling resolution on the predicted fatigue performance: modelling, experiment and simulation. *Metals.* 2021;11:822. doi:10.3390/MET11050822
- Schubnell J, Jung M, Le CH, et al. Influence of the optical measurement technique and evaluation approach on the determination of local weld geometry parameters for different weld types. *Weld World.* 2020;64(2):301-316. doi:10.1007/s40194-019-00830-0
- Fahrenwaldt HJ, Schuler V, Twrdek J. *Praxiswissen Schweißtechnik*. Springer Vieweg Wiesbaden; 2014. doi:10.1007/978-3-658-03141-1
- DIN EN ISO 5817:2014-6. *Schweißen—Schmelzschweißverbindungen an Stahl, Nickel, Titan und deren Legierungen (ohne Strahlschweißen)—Bewertungsgruppen von Unregelmäßigkeiten (ISO 5817:2014)*. 2014.



23. ISO 6520-1:2007. *Welding and allied processes—classification of geometric imperfections in metallic materials—Part 1: fusion welding*. 2007.
24. Volvo Group. STD 181-0004. Weld quality standard. 2016.
25. European Committee of Standardization. *Eurocode 9: Design of Aluminium Structures—Part 1-1: Structural Rules, 1999-1-1: 2007+A1*. European Committee of Standardization; 2009.
26. Zerbst U, Madia M, Schork B, et al. *Fatigue and Fracture of Weldments: The IBESS Approach for the Determination of the Fatigue Life and Strength of Weldments by Fracture Mechanics Analysis*. 1sted. Springer; 2018.
27. Renken F, von Bock und Polach RUF, Schubnell J, et al. An algorithm for statistical evaluation of weld toe geometries using laser triangulation. *Int J Fatigue*. 2021;149:106293. doi:10.1016/J.IJFATIGUE.2021.106293
28. Braun M, Neuhäusler J, Denk M, et al. Statistical characterization of stress concentrations along butt joint weld seams using deep neural networks. *Appl Sci*. 2022;12:6089. doi:10.3390/APP12126089
29. Kiyak Y, Madia M, Zerbst U. Extended parametric equations for weld toe stress concentration factors and through-thickness stress distributions in butt-welded plates subject to tensile and bending loading. *Weld World*. 2016;60(6):1247-1259. doi:10.1007/S40194-016-0377-X
30. Braun M, Kahl A, Willems T, Seidel M, Fischer C, Ehlers S. Guidance for material selection based on static and dynamic mechanical properties at sub-zero temperatures. *J Offshore Mech Arct Eng*. 2021;143(4):041704. doi:10.1115/1.4049252
31. Braun M, Kellner L. Comparison of machine learning and stress concentration factors-based fatigue failure prediction in small-scale butt-welded joints. *Fatigue Fract Eng Mater Struct*. 2022;45(11):3403-3417. doi:10.1111/FFE.13800
32. Braun M, Dörner A, Willems T, et al. Fatigue strength of fixed offshore structures under variable amplitude loading due to wind, wave, and ice action. In: *Proceedings of the ASME 2022 41st International Conference on Ocean, Offshore and Arctic Engineering. Volume 6: Polar and Arctic Sciences and Technology*. ASME; 2022. doi:10.1115/OMAE2022-78764
33. Schubnell J. *Experimental and Numerical Investigation of the Fatigue Performance of Notches and Welded Joints After High Frequency Mechanical Impact Treatment*. Karlsruhe Institute of Technology; 2021.
34. Gkatzogiannis S, Schubnell J, Knoedel P, Farajian M, Ummenhofer T, Luke M. Investigating the fatigue behaviour of small scale and real size HFMI-treated components of high strength steels. *Eng Fail Anal*. 2021;123:105300. doi:10.1016/J.ENGFAILANAL.2021.105300
35. Schubnell J, Ladendorf P, Sarmast A, Farajian M, Knödel P. Fatigue performance of high- and low-strength repaired welded steel joints. *Metals (Basel)*. 2021;11(2):293. doi:10.3390/met11020293
36. Dänekas C, Heikebrügge S, Schubnell J, Schaumann P, Breidenstein B, Bergmann B. Influence of deep rolling on surface layer condition and fatigue life of steel welded joints. *Int J Fatigue*. 2022;162:106994. doi:10.1016/J.IJFATIGUE.2022.106994
37. Anthes R, Köttgen V, Seeger T. Kerbformzahlen von Stumpfstoßen und Doppel-T-Stößen. *Schweißen und Schneid*. 1993;45(12):685-688.
38. Rainer G. *Errechnen von Spannungen in Schweißverbindungen mit der Methode der Finiten Elemente*. Technical University of Darmstadt; 1978.
39. Berge S. On the effect of plate thickness in fatigue of welds. *Eng Fract Mech*. 1985;21(2):423-435.
40. Madia M. IBESS user manual, version 1.2. 2019.
41. Jung M. *Entwicklung und Implementierung eines Algorithmus zur Approximation und Bewertung von Kerbfaktoren an Kehlnähten auf Basis berührungsloser 3D-Vermessung*. Karlsruhe Institut of Technology; 2018.
42. Ottersböck MJ, Leitner M, Stoschka M. Characterisation of actual weld geometry and stress concentration of butt welds exhibiting local undercuts. *Eng Struct*. 2021;240:112266. doi:10.1016/J.ENGSTRUCT.2021.112266
43. Konidena SK. *Digitization of weld geometry for fatigue life assessment by optical 3D measurement technique*. 2022.
44. DIN 50100-2016-12. Schwingfestigkeitsversuch—Durchführung und Auswertung von zyklischen Versuchen mit konstanter Lastamplitude für metallische Werkstoffproben und Bauteile. 2016.
45. Lecsek RL, Yee R, Lambert SB, Burns DJ. A probabilistic model for initiation and propagation of surface cracks in welded joints. *Fatigue Fract Eng Mater Struct*. 1995;18(7-8):821-831. doi:10.1111/J.1460-2695.1995.TB00907.X
46. Schubnell J, Discher D, Farajian M. Determination of the static, dynamic and cyclic properties of the heat affected zone for different steel grades. *Mater Test*. 2019;61(7):635-642. doi:10.3139/120.111367
47. Bäuml A, Seeger T, Boller C. *Material Data for Cyclic Loading, Supplement 1*. Elsevier; 1990.
48. Fiedler M, Wächter M, Varfolomeev I, Vormwald M, Esderts A. *FKM-Richtlinie: Rechnerischer Festigkeitsnachweis unter expliziter Erfassung nichtlinearen Werkstoffverformungsverhaltens Für Bauteile aus Stahl, Stahlguss und Aluminiumknetlegierungen*. 1sted. VDMA Verlag; 2019.
49. Lopez Z, Fatemi A. A method of predicting cyclic stress-strain curve from tensile properties for steels. *Mater Sci Eng A*. 2012;556:540-550. doi:10.1016/J.MSEA.2012.07.024
50. Berger C, Blauel JG, Hodulak L, Pyttel B, Varfolomeev I. *FKM-Richtlinie: Bruchmechanischer Festigkeitsnachweis für Maschinenbauteile*. 6thed. VDMA Verlag; 2006.
51. Tanaka K, Akiniwa Y. Resistance-curve method for predicting propagation threshold of short fatigue cracks at notches. *Eng Fract Mech*. 1988;30(6):863-876. doi:10.1016/0013-7944(88)90146-4
52. Zerbst U, Madia M, Beier HT. A model for fracture mechanics based prediction of the fatigue strength: further validation and limitations. *Eng Fract Mech*. 2014;130:65-74. doi:10.1016/J.ENGFRACMECH.2013.12.005
53. El Haddad MH, Smith KN, Topper TH. Fatigue crack propagation of short cracks. *J Eng Mater Technol Trans ASME*. 1979;101(1):42-46. doi:10.1115/1.3443647
54. Maierhofer J, Kolitsch S, Pippan R, Gänser HP, Madia M, Zerbst U. The cyclic R-curve—determination, problems, limitations and application. *Eng Fract Mech*. 2018;198:45-64. doi:10.1016/J.ENGFRACMECH.2017.09.032
55. ASTM. *ASTM E647-15e1 Standard Test Method for Measurement of Fatigue Crack Growth Rates*. ASTM International; 2015. Accessed: Apr. 03, 2023. [Online]. Available: <https://www.astm.org/e0647-15e01.html>

56. Wang X, Lambert SB. Stress intensity factors for low aspect ratio semi-elliptical surface cracks in finite-thickness plates subjected to nonuniform stresses. *Eng Fract Mech.* 1995;51(4): 517-532. doi:[10.1016/0013-7944\(94\)00311-5](https://doi.org/10.1016/0013-7944(94)00311-5)
57. Haibach E. *Betriebsfestigkeit: Verfahren und Daten zur Bauteilberechnung*. 3rd ed. Springer; 2006.
58. Hensel J, Nitschke-Pagel T, Dilger K. Engineering model for the quantitative consideration of residual stresses in fatigue design of welded components. *Weld World.* 2017;61(5):997-1002. doi:[10.1007/s40194-017-0467-4](https://doi.org/10.1007/s40194-017-0467-4)
59. Hensel J. Mean stress correction in fatigue design under consideration of welding residual stress. *Weld World.* 2020;64(3): 535-544. doi:[10.1007/s40194-020-00852-z](https://doi.org/10.1007/s40194-020-00852-z)

**How to cite this article:** Schubnell J, Konidena SK, Jung M, et al. Approach for the probabilistic fatigue assessment of welded joints based on the local geometry of the weld seam. *Fatigue Fract Eng Mater Struct.* 2023;1-20. doi:[10.1111/ffe.14170](https://doi.org/10.1111/ffe.14170)